

# A Parametric Analysis of Dissipation Capacity for $\Pi$ -type Floating Breakwaters

*Paolo Pezzutto, Piero Ruol, Luca Martinelli*

Department of Civil Arch and Environmental Eng. (ICEA), University of Padova  
Padova, Italy

## ABSTRACT

Aims of this work are to investigate the influence on wave energy dissipation for a  $\pi$ -type floating breakwater, according to non-dimensional variables.

The related FB dissipation coefficient distributions are examined with respect to two parameters: the first one is a geometric approximation of the wave period scaled with the heave natural motion period of the FB; the second is the wave steepness.

A Monte-Carlo based error analysis is carried out in order to evaluate the amount of error propagation involved in the derivation of dissipation coefficients.

Results show that the two invoked parameters appear to be the key for the description of the multiple processes here involved.

**KEY WORDS:** Transmission; Reflection; Energy Dissipation; Floating Breakwaters; Parametric Response; Bound Waves.

## INTRODUCTION

Transmission coefficient  $\tau$ , defined as transmitted to incident wave heights ratio, and reflection coefficient  $\rho$  (reflected to incident wave height ratio) are considered the most important parameters to define the efficiency of floating breakwaters (FB).

If we separate the radiated waves generated by the FB induced motion, we must argue that from a physical point of view, transmitted wave is what remains after the processes of reflection and dissipation. Actually, the shape of the incoming wave is first deformed due to partial reflection and possible breaking induced by the FB. The energy that is not reflected passes below and in some cases above (overtopping) the structure. In both cases some energy is dissipated.

We therefore think at energy loss (dissipation) as a key point to be investigated for a whole understanding of a FB efficiency problem.

The phenomena related to energy loss in passing a FB are somewhat difficult to be isolated and measured. Therefore, in order to account for that, a dissipation coefficient ( $\delta$ ), namely the ratio between a fictitious dissipated wave height and the incident one, has been introduced in literature (see e.g. Cox et al. 2007), being the result of straight energy equilibrium:

$$\delta^2 = 1 - (\rho^2 + \tau^2) \quad (1)$$

The errors on the analysis of wave transmission and reflection, even carried out with the most efficient techniques, are brought into the above computation, leading to high uncertainties in the dissipation process.

The design of a floating breakwater must be based on proper numerical and physical modelling in order to account for its performance and its interaction with the wave field. However, a simplified set of equations which approximate the FB behaviour or the comparison with results relative to similar structures may give to the engineer a reasonable starting point in the design process.

Recent efforts in this field has been made by Uzaki et al. (2011) and Ruol et al. (2012) who proposed simplified formulas, based on non dimensional parameters.

The results obtained by the authors through physical model tests may be compared with results relative to other structures on the basis of generalized parameters which avoid the dependence on single structures.

Based on the fact that wave transmission is mainly governed by the incoming wave period ( $T_p$ ) scaled by a FB characteristic natural motion period (heave -  $T_h$ ), Ruol et al (2012) propose a non-dimensional parameter  $\chi$ , which is similar to this ratio:

$$\chi = \frac{T_p}{2\pi} \sqrt{\frac{g}{d + 0.35w}} \approx \frac{T_p}{T_h} \quad (2)$$

The same set of data shows that even wave reflection and energy dissipation follow a generic law strongly depending on the latter parameter (Fig. 1).

However, their distribution may be “collapsed” into a single curve only considering at least another parameter which accounts for the wave breaking. Wave steepness, defined as the ratio of wave height ( $H$ ) over local wave length ( $L$ ), seems to be a valuable candidate.

Aims of this work are to investigate the sensitivity of dissipation coefficient distributions on the two proposed parameters ( $\chi$  and  $H/L$ ) for a  $\pi$ -type floating breakwater.

A set of experiments have been performed in a wave flume, on a  $\pi$ -type, chain moored, FB. Wave heights and periods arrays have been determined on the basis of the FB geometry, in the way that the parameters involved would span their respective range of validity across the critical region of  $\chi=1$ .

Only regular waves have been generated. This gives the opportunity to limit the uncertainties due to the separation of incident and reflected wave trains.

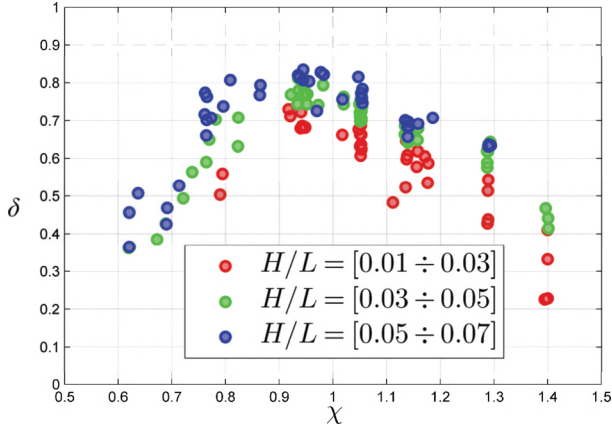


Fig. 1: Dissipation coefficients for different  $\pi$ -type floating breakwaters under irregular wave fields. Strong dependence on wave steepness is underlined by colours. In this case  $H/L$  is defined as significant wave height over wave length corresponding to spectral peak period.

## EXPERIMENTAL SET UP

Test have been carried out at the Maritime Laboratory of ICEA Department (University of Padova, IT)

The wave flume is 36m long, 1m wide and 1.4m deep. The rotating wave generator is equipped with an active absorption system. The flume ends with a gravel absorbing beach.

The floating breakwater model (Fig. 2) is a cylinder 0.98m long with a displacement of 56kg. The cross section width ( $w$ ) is 0.5m and its total height is 0.283m, including the three plates protruding downward. Draft ( $d$ ) is 0.178m. Its heave natural period, measured with a free decay test, is  $T_h=1.18s$ .

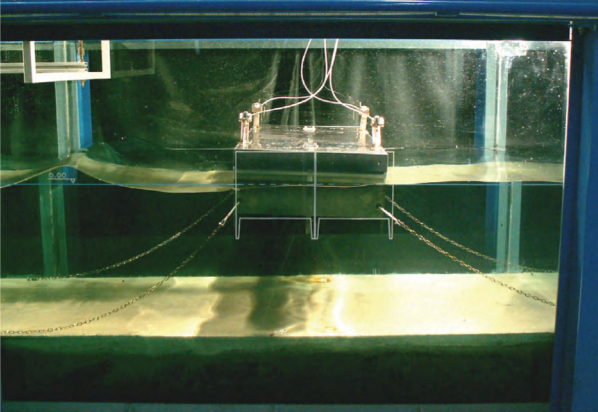


Fig. 2: The tested floating breakwater is not a pure  $\pi$ -type one, due to the three wings protruding downward. However, due to its behavior it must be classified as a  $\pi$ -type FB.

Waves have been generated with straight first order technique over 0.85m deep water, while the FB model was placed at depth  $d=0.80m$  on plane fixed bottom. The active absorbing system has been used for all tests. Shoaling and reflection phenomena which occur in the region between the paddle and the model are negligible, due to the almost flat bottom (0.5%). The FB has been moored with very loose chains. Test wave conditions have been designed in order to span a wide range

of both wave steepness and  $\chi$  parameter. The set can be divided into four series with fixed  $H/L$ . For each series eight wave periods were reproduced (Tab. 1).

Free surface elevations have been sampled at 20Hz with two resistive gauges arrays. Each array is build up with 4 in line gauges positioned 2.5m away from the initial position of the FB. This has been done in order to measure only well formed waves, preventing the sampling of evanescent mode disturbances. The first array spacing, relative to the first gauge is  $x-x_1=[0 \ 0.08 \ 0.26 \ 0.38] \ m$ . For the second array the relative spacing is the same:  $x-x_5=[0 \ 0.08 \ 0.26 \ 0.38] \ m$ .

Tab. 1: Test target wave conditions in terms of wave heights for different periods ( $T$ ) and wave steepness ( $H/L$ ). Target values of  $\chi$  are also reported.

$H/L$	0.01	0.03	0.05	0.07	$\chi$
$T [s]$					
0.8	0.01	0.03	0.05	0.07	0.67
0.9	0.01	0.04	0.06	0.09	0.76
1.0	0.02	0.05	0.08	0.11	0.84
1.1	0.02	0.06	0.09	0.13	0.92
1.2	0.02	0.07	0.11	0.15	1.00
1.3	0.03	0.08	0.13	0.18	1.09
1.4	0.03	0.09	0.14	0.20	1.17
1.5	0.03	0.10	0.16	0.23	1.26

## ERROR SOURCES

The method proposed by Zelt and Skjelbreia (1992) was used to separate incident from reflected waves. This method will be hereafter referred as ZS.

As mentioned in the introduction, the simple algebra of Eq.(1) hides some uncertainties, in fact:

$$\sigma^2(\delta^2) = \sigma^2(\rho^2) + \sigma^2(\tau^2) + 2 \text{cov}(\rho^2, \tau^2) \quad (3)$$

Moreover, the uncertainty on  $\tau$  depends on the coupling of two distinct ZS procedures. The first one, ZS1, is used to separate incident and reflected wave field at the first gauges array, thus getting an estimation of  $\rho$ . The second, ZS2, is used to separate the incident (transmitted with respect to the FB) and the beach reflected wave field. Only the combination of the two results allows evaluation of  $\tau$  as ratio between the two detected incident wave heights.

We compute reflection and transmission coefficients as ratios of  $0$ -th order spectral moments ( $m$ ) of the ZS separated signals:

$$\rho^2 = \frac{m_r}{m_i}, \quad \tau^2 = \frac{\bar{m}_i}{m_i} \quad (4)$$

where subscripts  $i$  and  $r$  stand for incident and reflected wave spectra, while  $\bar{m}_i$  identifies the incident signal on ZS2, namely the transmitted wave spectral moment, which is detected trough the application of ZS to the wake-side gauges recordings (gauges 5÷8). The first two moments ( $m_i$  and  $m_r$ ) are evaluated with ZS1 applied to gauges 1÷4. In the following subsections we discuss the main phenomena related to a wave flume pseudo-regular wave field which may lead to errors when analysing them through the single ZS procedure.

## Weak Non-Linearities

One of the error sources of ZS are the hypotheses on the wave field to be detected. In fact, ZS proceeds from a linear point of view, which leads to neglect existence of bounded components in the wave field. This traduces in errors in predicting components celerities of dispersive

waves, causing incorrect resolution of incident and reflected wave second (and higher) order components.

In order to have information both on the error of the method and on its uncertainties, we performed Monte-Carlo simulations generating synthetic signals of regular 2nd order Stokes waves time-series of the form:

$$\eta_n = (a \cos \theta_{i,n} + a_2 \cos 2\theta_{i,n}) + \rho(a \cos \theta_{r,n} + a_2 \cos 2\theta_{r,n}) \quad (5)$$

over  $N$  gauges placed at spatial coordinates  $\mathbf{x}=[x_1..x_N]$ . The phase angles at the  $n$ -th gauge of the incident ( $\theta_{i,n}$ ) and reflected ( $\theta_{r,n}$ ) wave may be recovered from

$$\begin{aligned} \theta_{i,n} &= \omega t - kx_n + \phi_{i,n} \\ \theta_{r,n} &= \omega t + kx_n + \phi_{r,n} \end{aligned} \quad (6)$$

Wave number  $k$  is the solution of linear dispersion relation of circular frequency  $\omega=2\pi f$  and water depth  $h$ . Incident and reflected waves are sampled at the  $n$ -th gauge with phase shifts  $\phi_{i,n}$  and  $\phi_{r,n}$  respectively. First order wave amplitude is  $a$ , and  $a_2$  its relative Stokes 2nd order wave amplitude.

The parameters for each realization are:  $a$ ,  $\phi_{i,1}$  and  $\phi_{r,1}$ . These are assumed to have uniform probability distribution and to be totally uncorrelated. Wave amplitude may therefore vary randomly between zero and a maximum which is related to  $\rho$ ; this is done in order to avoid high steepness and possible breaking in the gauges area. The incident wave phase ( $\phi_{i,1}$ ) accounts for the relative distance of the gauges from the wave generation point (wave generator) and  $\phi_{r,1}$  for the gauges relative position from the reflecting obstacle. Hence they are assumed to vary randomly in the range  $[-\pi, \pi]$ .

A number of realizations have been performed for each couple of known variables  $(\omega, \rho)$  until convergence on the mean reflection coefficient relative error  $\varepsilon_r = \rho_{ZS} / \rho - 1$  ( $\rho_{ZS}$  is the Zelt and Skjelbreia (1992) evaluated reflection coefficient and  $\rho$  its true value) and its other first 3 distribution moments (variance, skewness and kurtosis).

We report here an example of application of this MC procedure. Water depth is  $h=0.80m$ , gauge spacing is  $\mathbf{x}-x_1=[0 \ 0.08 \ 0.26 \ 0.38] m$ . The latter is a design condition to properly resolve waves with frequencies in the range of  $[0.8, 1.2]Hz$  with ZS.

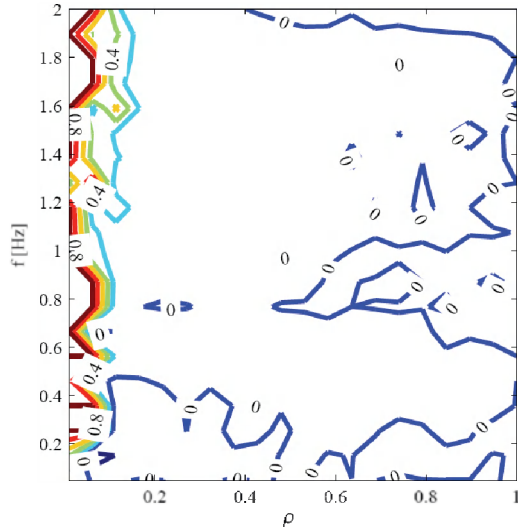


Fig. 3: Results of a Monte-Carlo simulation. Relative error ( $\varepsilon_r = \rho_{ZS} / \rho - 1$ ) in estimating reflection coefficient ( $\rho$ ) by Zelt and Skjelbreia (1992) procedure on a second order Stokes wave. Gauges spacing relative to first gauge is  $[0 \ 0.08 \ 0.26 \ 0.38] m$ , water depth  $h=0.80m$ .

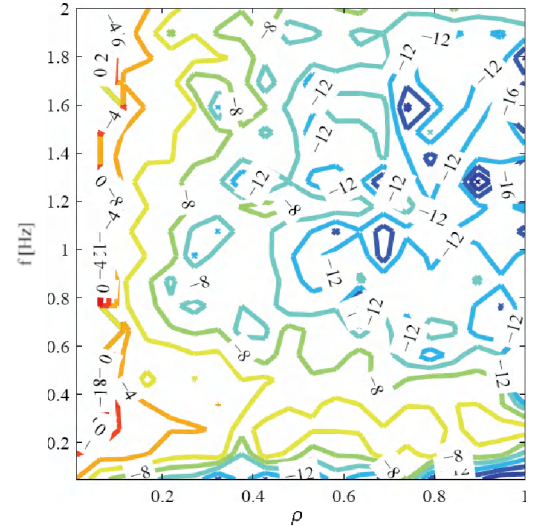


Fig. 4: Results of a Monte-Carlo simulation. Error variance plotted as  $\log_{10}[\sigma^2(\varepsilon)]$ . Same conditions of Fig.2.

For reflection coefficients higher than  $0.1$ , the relative error is negligible (Fig. 3) as well as its uncertainty (Fig. 4). However, for small  $\rho$  ( $\rho < 0.1 \div 0.2$ )  $\varepsilon_r$  grows up to  $0.8 \div 1$  and the  $\sigma(\varepsilon_r)$  appears to be of the same order.

We must point out that no errors appear when evaluating reflection coefficients considering only a narrow band around the carrier frequency  $\omega$ . No graphics are reported to show this trivial result.

Proceeding from that, one may assume that for our practical purposes it is sufficient to filter the signals acquired by each gauge with an ideal filter. This will be designed in order to pass the first harmonic band only. Then we apply ZS to separate incident and reflected wave with very small error and uncertainty. Filtering after applying ZS would lead to approximately the same result.

### Pseudo-Regular Waves in a Flume

What we do measure in a flume is pretty far from Eq.(5). The way of generating the waves and the shape of the reflecting obstacle would lead to the release of waves which travel at their own celerity, with a wavenumber  $k_F$  which is the solution of the linear dispersion relation of their own circular frequency. Subscript "F" stands for "free" wave.

In quasi-regular wave fields interacting with structures it is therefore common to sample, at the  $n$ -th gauge, a signal of the form:

$$\begin{aligned} \eta_n &= a \cos \theta_{i,n} + a_2 \cos 2\theta_{i,n} + b_2 \cos \vartheta_{i,n} \\ &+ \rho_1 a \cos \theta_{r,n} + \rho_1 a_2 \cos 2\theta_{r,n} + \rho_2 b_2 \cos \vartheta_{r,n} \end{aligned} \quad (7)$$

where the phases of the non-harmonic component with amplitude  $b_2$  are defined as follows

$$\begin{aligned} \vartheta_{i,n} &= 2\omega t - k_F x_n + \phi_{i,n} \\ \vartheta_{r,n} &= 2\omega t + k_F x_n + \phi_{r,n} \end{aligned} \quad (8)$$

phase shifts ( $\phi_{i,n}$  and  $\phi_{r,n}$ ) differs from the harmonic component ones, and  $\rho_2$  is the reflection coefficient associated to the free component.

We must add that in an unreliable wave field, in which  $a_2$  is set equal to zero, *i.e.* no bounded components are travelling in any direction, ZS is able to detect exactly incident and reflected waves. This comes out from the linearity hypotheses of the method, that is to say that ZS considers each perturbation as a free wave.

When attempting the generation of pseudo-regular waves the release of these free components can be avoided, thus generating more-regular waves (see *e.g.* Schaffer, 1996). On the other hand, as we mentioned before, the general process around the reflecting obstacle is such that non-harmonic waves, travelling backwards, are liberated from that region. This occurs especially (but not only) in the case of waves interacting with floating bodies.

### Near-Resonant Interactions

The last thing that we must point out is that in case of relatively high-energetic second order components (both  $a_2$  and  $b_2$  not negligible with respect to  $a$ ) the wave pattern along the flume does not remain constant. By a linear point of view, being the celerity of the non-harmonic component lower than that of the carrier, the wave profile will vary periodically in space with a beat length  $L_B=2\pi/(k_F-2k)$ , as it can be deduced directly from Eq.(7). But what is of our interest here is the non-linear point of view: the amplitudes of the three components oscillate in the propagation direction according to the same beat length based spatial distribution. This is due to what in literature is known as “*triad interaction*” (see *e.g.* Madsen and Sørensen, 1993).

If the gauges spacing is too large ( $x_N-x_I=O(L_B)$ ), then the amplitudes evolution leads to wrong interpretation of the motion field. That is to say that these amplitude variations are interpreted by the signal solving method (ZS in this case, but for another linear method would be the same) as due to partial reflection.

For our practical purposes, we are not taking these phenomena into account, shifting that as a target for future analyses. By doing that we are aware that an amount of error is not included in our estimations.

However, since we are using a fixed array for the whole set of laboratory tests, some considerations may be added.

We know that exchange between three interacting wave modes become relevant for shallow and intermediate water depths (Madsen and Sørensen, 1993). Therefore, in the case of long waves (intermediate water depth), we consider the designed gauge spacing sufficiently small to not experience considerable amplitude variation of the wave components between the  $N$  gauges. For short waves (deep water) interactions do not occur.

### Other Error Sources

By an idealistic 2DV point of view everything may be fine so far. But we made hypotheses that might not be fully satisfied in a laboratory.

Wave flume near resonant frequencies might be avoided when attempting the generation of pseudo-regular waves. In fact, for these wave fields, due to the regular forcing of the paddle, these near-resonant phenomena enhance in magnitude, corrupting the entire experiment. This does not happen for most irregular wave fields (Gronbech et al., 1996).

However, in some cases the tests might be done, and there may be no way of changing the facility. Hence, these aspects must be taken into account, controlling their magnitude when possible, and recognised when analysing the sampled data.

### ERROR ESTIMATION

Filtering the signals passing only a narrow band centred at the principal component frequency  $\omega$ , as proposed before, would not be a correct procedure. Therefore, being aware that some energy is carried back from the reflecting obstacle by the non-harmonic component ( $2\omega$ ), we have processed signals which have the form of Eq.(7). This procedure is a source of errors due to the presence of bounded harmonics which travels at the same carrier celerity.

### Monte-Carlo Approach

We performed Monte-Carlo (MC) simulations based on Eq.(7),

considering the following 6 parameters:  $a$ ,  $\rho_I$ ,  $\varphi_{i,1}$ ,  $\varphi_{r,1}$ ,  $\phi_{i,1}$  and  $\phi_{r,1}$ . An amount of energy is supposed to be carried back by the non-harmonic component, but this value is limited by fixing a coefficient  $\beta$  such that  $\rho_I$  is a uniformly distributed random variable in the interval:

$$\rho_I \in [(1-\beta)\rho, \rho] \in \mathfrak{R} \quad (9)$$

being  $\rho$  the total reflection coefficient. For the free component,  $\rho_2$  is a function of  $\rho$  and  $\rho_I$ , satisfying the following condition:

$$\rho^2 = \frac{\rho_I^2(a^2 + a_2^2) + \rho_2^2 a_2^2}{a^2 + a_2^2 + a_2^2} \quad (10)$$

Second order amplitudes are known on the basis of Stokes-like solutions, provided that  $a$  is fixed (see Schaffer, 1996). The latter is a uniformly distributed random variable in the interval  $[a_{min}, a_{max}]$  which is defined for each case on the basis of the sampled time-series. We report in Fig. 5 a typical distribution of the MC output.

Results of this procedure are used to estimate errors and uncertainties of the ZS detected values in processing laboratory data.

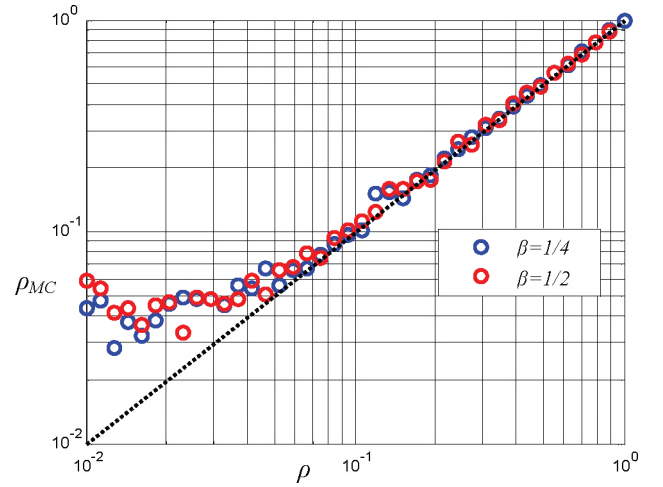


Fig. 5: Expected ZS values for reflection coefficient  $\rho_{MC}$  based on MC simulations with time-series of the kind Eq.(7). Parameters are  $a$ ,  $\rho_I$ ,  $\varphi_{i,1}$ ,  $\varphi_{r,1}$ ,  $\phi_{i,1}$  and  $\phi_{r,1}$ .  $b_2$  is the paddle generated free wave amplitude. Fundamental frequency is  $f=1\text{Hz}$ .  $\beta$  accounts for  $\rho_2$  magnitude providing that  $\rho=m_r/m_i$ .

The evaluation of  $\rho$  and  $\tau$  will be done, for each test, in the following way.

We process first gauges array samples, obtaining an initial value for the reflection coefficient:

$$DATA\{I:4\} \xrightarrow{IN} ZS1 \xrightarrow{OUT} \rho_{ZS1} \quad (11)$$

With this estimation we enter a curve of the kind depicted in Fig. 5, *i.e.* we perform a series of MC simulations, looking for the best match between  $\rho_{MC}$  and  $\rho_{ZS1}$ , obtaining the most probable true value of  $\rho$  and the associated distributions of the incident and reflected spectral moments:

$$\rho_{ZS1} \xrightarrow{IN} MC \xrightarrow{OUT} \{\rho, \sigma^2(\rho), m_i, m_r\} \quad (12)$$

Afterwards we do the same with respect to the second gauges array:

$$DATA\{5:8\} \xrightarrow{IN} ZS2 \xrightarrow{OUT} \rho_{ZS2} \quad (13)$$

In this case we are interested in storing the distribution of the incident  $0$ -th spectral moment only:

$$\rho_{ZS2} \xrightarrow{IN} MC \xrightarrow{OUT} \bar{m}_i \quad (14)$$

We can then compute the transmission coefficient:

$$\tau^2 = \frac{E(\bar{m}_i)}{E(m_i)}, \quad (15)$$

where  $E(X)$  stands for the expected value of  $X$ . Its variance can be estimated as:

$$\sigma^2(\tau^2) = \tau^4 \left[ \frac{\sigma^2(\bar{m}_i)}{\bar{m}_i^2} + \frac{\sigma^2(m_i)}{m_i^2} - 2 \frac{E(m_i \bar{m}_i)}{m_i \bar{m}_i} + 2 \right] \quad (16)$$

The covariance associated to transmission and reflection coefficients is:

$$\text{cov}(\rho^2, \tau^2) = 2 \left[ E\left(\frac{\bar{m}_i m_r}{m_i^2}\right) - E\left(\frac{\bar{m}_i}{m_i}\right) E\left(\frac{m_r}{m_i}\right) \right] \quad (17)$$

Finally, the uncertainty on the dissipation coefficient is evaluated with Eq.(3).

## RESULTS

Data are plotted according to the proposed parameterisation ( $\chi, H/L$ ). Each graphic will be presented in the same manner, except where indicated. In order to underline their energetic meaning, the square of the coefficients is used, instead of the straight wave ratios.

### Reflected Wave Energy

Next figure (Fig. 6) reports the reflection coefficients evaluated with ZS method for the whole dataset.

Reflection coefficients are evaluated with a single ZS procedure (on gauges 1÷4). The uncertainties are therefore evaluated in terms by MC simulations (12).

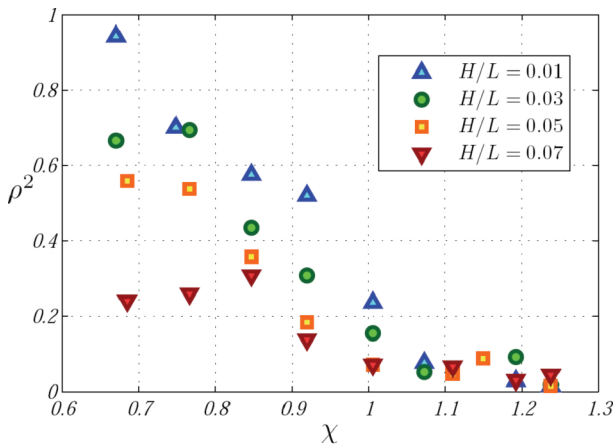


Fig. 6: ZS computed reflection coefficients.

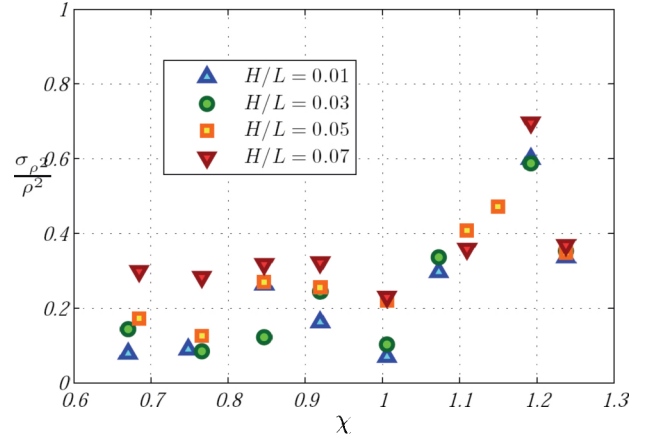


Fig. 7: Monte-Carlo based error estimation on single ZS performance; normalized standard deviation for  $\rho^2$ .

### Transmitted Wave Energy

We here report the joined results of the coupled ZS analyses on the signals sampled at the two gauges arrays. Transmission coefficients (Fig. 8) are computed as ratios of the second array (gauges 5÷8) incident wave height over the first array (gauges 1÷4) one. The confidence (Fig. 9) is then evaluated throughout Eq.(16).

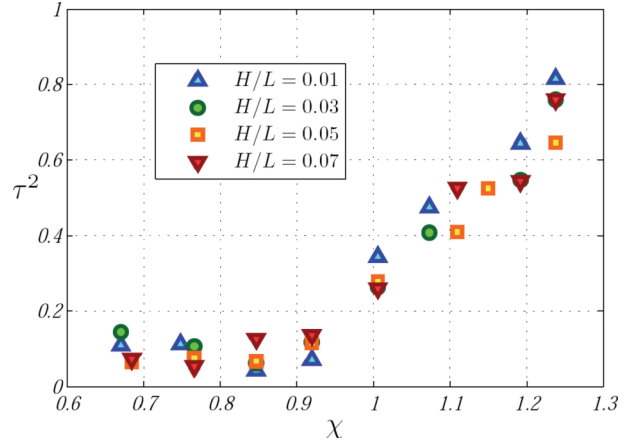


Fig. 8: Coupled ZS computed transmission coefficients.

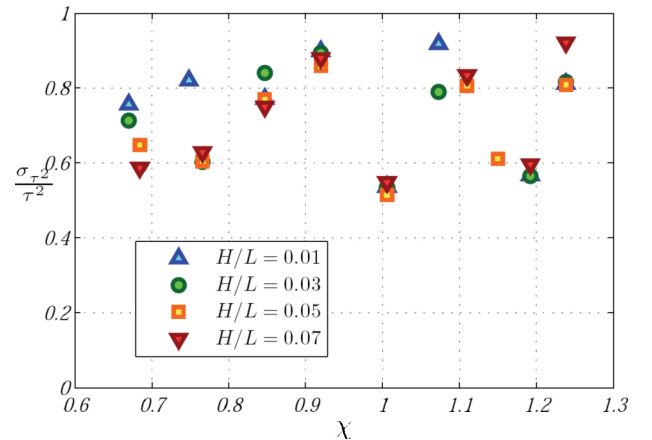


Fig. 9: Monte-Carlo based error estimation on coupled ZS performances; normalized standard deviation for  $\tau^2$ .

### Dissipated Wave Energy

The next three figures report the dissipation coefficients (Fig. 10), their

evaluated uncertainties (Fig. 11) and a close up view to the range of the acceptable data, for the two extreme wave steepness series, including the respective ranges of confidence (Fig. 12).

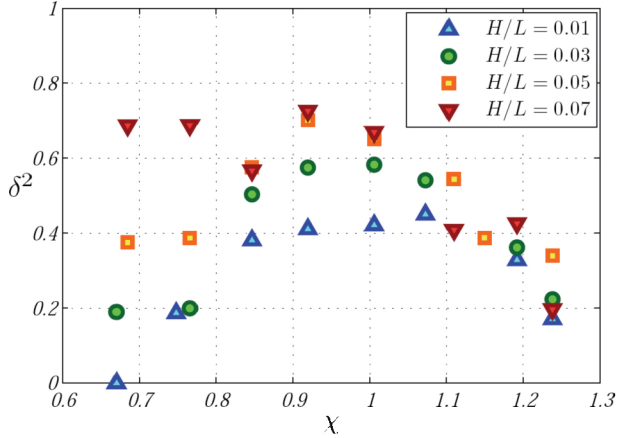


Fig. 10: Dissipation coefficients computed as Eq.(1), straight energy equilibrium.

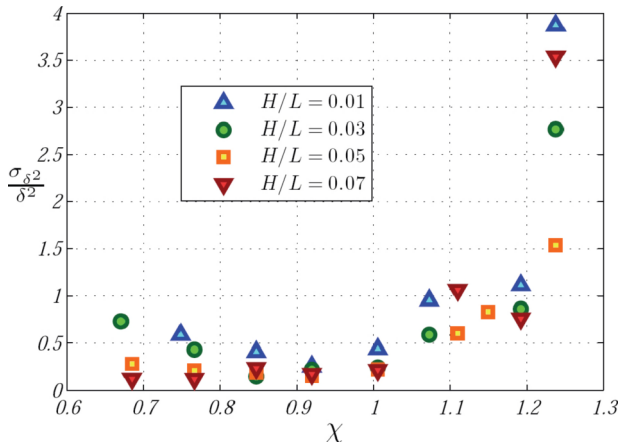


Fig. 11: Monte-Carlo based error estimation on coupled ZS performances; normalized standard deviation for  $\delta^2$ . Error propagated according to Eq.(3).

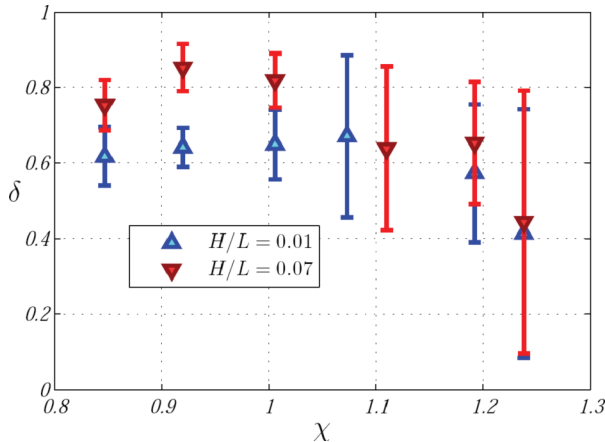


Fig. 12: Dissipation coefficients for the two extreme wave steepness series and  $\chi > 0.8$ . Error bars are standard deviations for  $\rho$ :  $\sigma(\rho) \approx \sigma(\rho^2)$ .

### Additional Observations

During the laboratory tests we recorded a list of information based on visual analysis of the wave field. These are mainly related to wave

breaking and FB overtopping. The following Tab. 2 reports these useful observations.

Tab. 2: 2DV dissipating phenomena: wave breaking (*N*:none, *S*:spilling-like breakers, *P*:plunging-like) and FB overtopping (*A*:none, *D*:water on deck, *J*:water jet)

<i>H/L</i>	0.01	0.03	0.05	0.07	$\chi$
<i>T</i> [s]					
0.8	<i>N-N</i>	<i>N-N</i>	<i>N-N</i>	<i>S-N</i>	0.67
0.9	<i>N-N</i>	<i>N-N</i>	<i>N-N</i>	<i>S-N</i>	0.76
1.0	<i>N-N</i>	<i>N-D</i>	<i>S-N</i>	<i>P-D</i>	0.84
1.1	<i>N-N</i>	<i>N-D</i>	<i>S-D</i>	<i>P-J</i>	0.92
1.2	<i>N-N</i>	<i>S-D</i>	<i>S-J</i>	<i>P-J</i>	1.00
1.3	<i>N-N</i>	<i>S-N</i>	<i>P-J</i>	<i>P-J</i>	1.09
1.4	<i>N-N</i>	<i>N-N</i>	<i>S-D</i>	<i>P-J</i>	1.17
1.5	<i>N-N</i>	<i>N-N</i>	<i>S-N</i>	<i>S-D</i>	1.26

Another dissipative phenomenon we observed was the growth of noisy macro-vortices at FB sides (flume walls) under waves steepness  $H/L=0.03$ , and wave periods close to  $1.1 \div 1.2s$ .

We noticed some distortions of the 2DV expected wave field. In some cases a channel cross mode was excited by the combined regular forcing of the paddle and FB motion. That occurred for wave periods close to  $0.8 \div 0.9s$ , *i.e.* wavelengths close to flume width.

Some asymmetries were enhanced during testing wave conditions with periods in the interval  $0.9 \div 1.1s$ . These became visible after approximately  $40 \div 60s$  from the beginning of the test. This has been taken into account when analyzing data records, cutting all the time-series at the point these instabilities show up.

### DISCUSSION

The enhancement of resonant cross modes at low periods severely affect results below  $\chi=0.8$ . Even if the relative points in the plots follow general trends, we must discard them from the quantitative point of view.

### Uncertainties

The expected errors done when analysing pseudo-regular waves throughout ZS procedure are acceptable. The statistical Monte-Carlo analysis shows that relative errors become important when  $\rho < 0.1$  (Fig. 3, Fig. 5). For the present experimental set-up it appears that no reflection coefficients smaller than  $0.05$  can be detected, considering a weak non-linear wave field.

The worse conditions, by this point of view, match the cases in which both gauges arrays meet small reflection coefficients, *i.e.* very long waves (and an almost perfectly absorbing beach). These situations are very far from the FB working region.

On the other hand, when taking into account the uncertainties of the method, things appear slightly different.

The single ZS procedure become worse as the period of the incoming wave grows, and, for  $\chi < 1$ , wave steepness plays a fundamental role (Fig. 7). Uncertainties spread vertically in accordance with the reflection coefficient distribution (Fig. 6). Anyhow, the relative standard deviation of  $\rho^2$  lies almost under  $50\%$ , which means approximately  $25\%$  if we account for  $\rho$ .

But, when coupling two ZS procedures, in order to compute wave transmission, the expected deviations on  $\tau^2$  grows up to  $80\%$  (Fig. 9). This makes the uncertainties on the dissipated wave energy explode for relatively long waves, due to Eq.(3). However, in the critical region  $\chi \in (0.8; 1.1)$ , we end up with an almost acceptable  $50\%$  of uncertainties on our results (Fig. 11).

We also observe that for  $\chi > 0.8$ , coinciding with the acceptable data, the relative standard deviations of the transmission coefficients are almost

insensitive to wave steepness. This is probably due to  $\tau^2$  general behaviour (Fig. 8). In the case of dissipation, they again slightly spread out.

### Dependence on $\chi$

The parameter introduced by Eq.(2) governs the overall process of energy transmission (Fig. 8), as observed by Ruol et al. (2012). As  $\chi$  grows the transmitted energy grows, and the amount of reflected energy decreases (Fig. 6).

The maximum of dissipated energy falls in the near-resonant region  $\chi \approx 1$  (Fig. 10) and the general trend can be accepted due to the relatively small uncertainties.

### Dependence on wave steepness

Wave steepness plays a fundamental role in the region below  $\chi \approx 1$ .

Except for energy transmission, which is practically insensitive to this parameter, the steeper the wave, the lower the amount of energy reflected back to the open sea. This is due to the enhancement of the dissipative phenomena.

Even if the uncertainties cannot be neglected, the general trend in the dissipation coefficients shows that steeper waves dissipate more energy. This aspect is enhanced in the region  $\chi \in [0.8; 1]$  (Fig. 10 and Fig. 12), despite the strongest observed dissipation phenomena occurs for slightly longer waves  $\chi \approx 1.1$  (Tab. 2). In this second region, we were expected to find a secondary maximum, and we found it only for the less steep waves, which coincide with the macro-vortices reported in "Additional Observations" section.

If we are allowed to neglect the uncertainties we may argue that as the wave steepness grows, the peak in the  $\delta$  distribution moves from right to left: from  $\chi \approx 1.1$  for  $H/L \approx 0.01$  to  $\chi \approx 0.9$  for  $H/L \approx 0.07$ . The reason for that may be a shift in the most dissipative agent: from vorticity in the inner fluid region, to vorticity due to the breakers, even before the impact with the FB.

### CONCLUSIONS

We have investigated the dissipative interactions of a  $\pi$ -type Floating Breakwater with 2DV pseudo-regular wave fields.

Two parameters were identified to be of major importance to investigate on the multiple processes involved. The first one ( $\chi$ ), introduced by Ruol et al. (2012), is a measure of the incoming wave period, normalised with the heave natural period of the FB. The second parameter is the incoming wave steepness ( $H/L$ ).

We run a series of laboratory experiments spanning a useful range for both parameters.

Incident and reflected wave fields have been separated by Zelt and Skjelbreia method together with a Monte-Carlo based analysis. This helped us to account for the error propagation due to the algebra involved when computing dissipation coefficients.

Beyond the method uncertainties we can conclude that the two invoked parameters lead to explain the overall general behaviour of the FB.

In particular,  $\chi$  appears to govern the main distribution of energy reflection, transmission and dissipation. Moreover, in the critical region,  $\chi \approx 1$ , the latter shows a relative peak. This enhances for growing wave steepness.

### ACKNOWLEDGEMENTS

The support of the European Commission through Contract 244104 THESEUS ("Innovative technologies for safer European coasts in a changing climate"), FP7.2009-1 Large Integrated Project, is gratefully acknowledged.

### REFERENCES

- Cox, R., Coghlan, I., Kerry, C., 2007, "Floating breakwater performance in irregular waves with particular emphasis on wave transmission and reflection, energy dissipation, motion and restraining forces", *Proc. Int. Conf. Coastal Structures 2007*, Vol 1, pp 351-362.
- Grønbech, J., Jensen, T., Andersen, H., 1996, "Reflection analysis with separation of cross modes", *Proc. 25th Int. Conf. Coastal Engng.*, pp 968-980.
- Madsen, P. A., and Sorensen, O. R., 1993, "Bound waves and triad interactions in shallow water", *Ocean Engng.*, Vol 20, No 4, pp 359-388.
- Ruol, P., Martinelli, L., Pezzutto, P., 2012, "Formula to Predict Transmission for  $\pi$ -type Floating Breakwaters", accepted, *Journal of Wat. Port Coastal and Ocean Engng.*
- Uzaki, K., Ikehata, Y., Matsunaga, N., 2011, "Performance of the Wave Energy Dissipation of a Floating Breakwater with Truss Structures and the Quantification of Transmission Coefficients", *Journal of Coastal Research*, Vol 27, No 4, pp 687-697.
- Schäffer, H. A., 1996, "Second order wavemaker theory for irregular waves", *Ocean Engng.*, Vol 23, No 1, pp 47-88.
- Zelt, J.A. and Skjelbreia, J.E., 1992, "Estimating incident and reflected wave fields using arbitrary number of wave gauges", *Proc. 23rd Int. Conf. Coastal Engng.*, pp 777-789.